Passive UHF-RFID Hyperbolic Positioning of Moving Tags by Exploiting Neural Networks

Spyros Megalou, Aristidis Raptopoulos Chatzistefanou, Anastasios Tzitzis, Traianos V. Yioultsis, *Member, IEEE,* and Antonis G. Dimitriou, *Senior, IEEE*

***Abstract*—In this paper we propose a novel real-time tracking method of a moving UHF-RFID tag. The purpose is to track the interests of RFID-tagged visitors inside a museum from a set of fixed antenna-installations. Two antenna pairs collect phase-measurements from the target tag. Phase differences are calculated for each pair and then mapped to distance-differences of the target-tag from the two antennas. The latter corresponds to a hyperbola for each pair of antennas. The intersection of the two hyperbolas denotes the position of the tag. The cross section of the hyperbolas is derived by a trained neural network. The proposed method neither requires knowledge of the tag's initial position nor the trace followed (e.g. conveyor belt). Its computational complexity allows for real-time applicability. Experiments were conducted inside multipath-rich laboratory environments. Two types of experiments were conducted to validate the performance of the algorithm. Firstly a tag was placed on a moving robot, which estimated its own position at cm accuracy, thanks to its lidar sensor, representing the ground truth. Secondly a tag was placed on an ArUco Marker which was carried by a human following various trajectories. The proposed method achieved tracking with mean error under 0.5m throughout the experimental campaigns.**

***Index Terms*—RFID, tracking, hyperbolic positioning, phase, neural network.**

I. Introduction

FOURTH Industrial Revolution is starting to change our everyday life in a lot of its aspects. On this ongoing automation of traditional manufacturing, processing of goods, and industrial practices, Radio Frequency Identification (RFID) technology plays a significant role. An important part of RFID in this revolution is the localization and tracking of objects or humans. From tagging goods and empowering logistics operations, to tagging humans and enhancing security or providing statistics of visiting patterns, finding ways to track a moving RFID tag is of great importance.

In this paper the objective is to track a visitor in the Archaeological Museum of Thessaloniki. Upon entrance, the visitors are given a ticket with an attached RFID tag. Antennas and readers are set at known locations in the museum collecting phase and RSSI measurements associated with each RFID tag. The phase data are exploited to track the moving tag, thus quantifying the behavior of visitors and providing statistics of interest per exhibit helping the administration to improve the experience of visitors.

RFID tag tracking has been investigated in prior art. In [1], [2] and [3] "Received Signal Strength Indicator" (RSSI) data are exploited to track the tag. RSSI is not a reliable indicator due to the fact that power is heavily influenced by environmental factors, introducing multipath and shadowing, thus reducing the accuracy of the positioning.

Other methods such as [4], [5] and [6] take advantage of Angle Of Arrival (AOA) data, calculated from measurements collected from multiple antennas. In [4] the trace of the tag is known a priori, as the authors track the tag on a conveyor belt while in [5] the authors surround the target tags with three prototype antenna arrays to localize the tag. In [6], the authors aim to identify the "trace" of an "RFID" pen in space, in order to identify "letters" or entire "words", by successively treating measured phase differences between closely (poor resolution - no grating lobes) and sparsely (high resolution with grating lobes) spaced antennas.

Authors in [7], [8] and [9] exploit phase measurements to track a moving tag. However the initial position of the tag must be known beforehand. Tagoram [10] and [11] are methods that exploit the Phase-Of-Arrival (POA) of the signal to localize a moving tag. However, both methods consider a calculations' grid; posing a trade-off between accuracy and execution-speed. In [12], measurements from a prototype bistatic, synchronized transceiver are necessary, where the Tx and Rx antennas are misplaced in order to surround the tracked area.

In [13] - [16] device-free tracking methods are proposed. The targets neither carry equipment nor tags and the authors exploit the effect of multipath to perform localization and tracking. In a different approach, a wireless sensor network (WSN) grid is used in [17], [18] to track a non-tagged target. All the device-free tracking methods have the major drawback of not recognizing the ID of the tracked target and can hardly track two or more targets.

"Hyperbolic positioning", [19], [20] and [21], refers to methods that exploit phase differences measured from known positions, since the locus of each measurement corresponds to a hyperbola. In such methods, the cross section of two hyperbolas would result in an estimated position of the tag. When multiple antennas are involved, the estimation is improved. This principle is exploited in [19] and [21], where movement of the antenna at known positions results in accurate estimations of the position of a *static* tag. Furthermore, both [20] and [21] provide methods or closed-form expressions where the intersection of two hyperbolas is calculated exactly,

Manuscript received Oct 29, 2021.

This research has been co-financed by the European Union and Greek national funds through the Operational Program Competitiveness, Entrepreneurship and Innovation, under the call RESEARCH – CREATE – INNOVATE (project code:T2EDK-02000).

The authors are with the School of Electrical and Computer Engineering, Aristotle University of Thessaloniki, 54124 Thessaloniki, Greece (e-mail: antodimi@ece.auth.gr).

under the constraint that the antennas and the tag belong to the same plane. In the general case the pair of antennas could be installed anywhere in the search volume, thus forming hyperbolas with rotated major axes along random 3D directions, which cannot be solved by the expressions in [20], [21].

With respect to prior art, we aim to develop a tracking method that avoids the calculations on a grid, [10], [11] and [6], in order to be applicable in real-time for any problem, regardless of the size of the search space. Phase is chosen over RSSI, [1], [2] and [3], as a more reliable indicator. AOA methods [5] also consider the phase difference measured at two known positions, but are based on the assumption that the target is far from the antennas, so that the Line-Of-Sight paths from the tag to the antenna-elements are parallel. Hyperbolic positioning identifies the exact location of the tag and can be applied directly on the collected data, but may not be applied in random 3D antenna-installations.

In this work, we propose a tracking method that is based on hyperbolic positioning. At least two antenna-pairs are fixed at known positions, collecting phase measurements from a moving RFID tag. Phase differences are calculated for each pair and then mapped to distance-differences of the two antennas from the target tag. To overcome the limitation of calculating cross-sections of 3D hyperbolas along another plane, we introduce the idea of training a neural network for any given geometry. A neural model is trained to approximate a function that maps all possible phase-differences from antenna-pairs to a unique position of the target tag. After the training phase, application of the method is rapid; i.e. when the trained network is given any set of phase measurements, it instantly outputs the position of the tag. Furthermore, in contrast to prior-art, related to "hyperbolic positioning", where multiple antennas localize a fixed tag, we evaluate whether few antennas can track a moving tag. As a result, emphasis is given on processing series of measured data, to filter out the expected phase-noise related to the measurements and applying Kalman filtering on the resulting data. The proposed method is experimentally verified in two setups; the first involves a robot, in order to accurately acquire the ground truth of its trace and the second involves a person, whose actual position is estimated by a visual tracking system. In the 8 experiments, the mean error ranges from 24cm to 47cm and the standard deviation between 17cm to 33cm.

The paper is organized as follows. The method is presented in Section II. Simulation results are given in Section III. Comparison with experimental data is presented in Section IV and the conclusions in Section V.

II. Proposed Localization Method

The proposed method tracks a moving RFID tag. Two antenna pairs (4 antennas in total) are fixed at known locations. The RFID reader interrogates the tag and reports the phase of the backscattered signal. The principle of the proposed method is summarized below:

1) Phase measurements from all antennas are collected. The phase differences for each antenna pair are calculated and unwrapped. As a result, two phase-difference curves are created with respect to time.
2) The unwrapped phase measurements are filtered, to discard the expected phase noise.
3) For a given time, the recorded phase-difference from each antenna pair is mapped to distance-difference of the two antennas from the target tag. The latter corresponds to a hyperbola for each pair of antennas, where the locations of the antennas represent the foci of each hyperbola.
4) The cross section of the hyperbolas for any given time represents the estimated location of the tag at the specific time. We introduce a neural network (NN), which has been trained beforehand for the specific geometry. The NN takes the phase-differences from each antenna pair as input and outputs the expected position of the tracked tag rapidly.

A. Data Collection and Processing

The phase reported for each antenna i is wrapped and can be expressed as [22]:

$$\phi_i = (\phi^i_{prop} + \phi^i_o + \phi^i_{noise}) mod(2\pi), \tag{1}$$

$$\phi_{noise} \sim \mathcal{N}(0,\, \sigma^2_{phase})\,. \tag{2}$$

where i is the index for each antenna (i.e. 1, 2, 3 and 4), ϕ^i_o is the phase offset including phases of the cables and other hardware and ϕ^i_{noise} is the measurement's noise. Phase ϕ^i_{prop} corresponds to the phase accumulated due to the round trip of the electromagnetic wave, $||\mathbf{A}_{tag} - \mathbf{A}^i_{ant}||_2$, and is given by:

$$\phi^i_{prop} = \frac{4\pi}{\lambda}||\mathbf{A}_{tag} - \mathbf{A}^i_{ant}||_2 = \frac{4\pi d_i}{\lambda}, \tag{3}$$

$$||\mathbf{A}_{tag} - \mathbf{A}^i_{ant}||_2 = \sqrt{(x_{tag} - x_i)^2 + (y_{tag} - y_i)^2}, \tag{4}$$

where $\mathbf{A}_{tag} = [x_{tag}, y_{tag}]$ denotes the location of the tag, $\mathbf{A}^i_{ant} = [x_i, y_i]$ denotes the i-th antenna's location, λ is the wavelength of the electromagnetic field, and $d_i \equiv ||\mathbf{A}_{tag} - \mathbf{A}^i_{ant}||_2$ the Euclidean distance between the i-th antenna and the tag.

For each antenna pair the difference of the two phases is calculated. Let $\Delta\phi_{12,t}$ and $\Delta\phi_{34,t}$ denote the phase difference between antenna 1-2 and 3-4 accordingly, at time t:

$$\Delta\phi_{12,t} = \phi_{1,t} - \phi_{2,t} \quad \text{and} \quad \Delta\phi_{34,t} = \phi_{3,t} - \phi_{4,t} \tag{5}$$

Due to the wrapped nature of the phase measurements, ambiguities regarding the accurate calculation of the phase differences arise. In the following subsections we elaborate on these ambiguities and present solutions to overcome them.

1) Phase difference range: The range of phase difference of an antenna-pair, depends on the distance between the two antennas. Considering unwrapped phase measurements and a noise/multipath free scenario by substituting (3) in (5) for antenna pair 1-2:

$$\Delta\phi_{12} = \frac{4\pi}{\lambda}(d_1 - d_2) \tag{6}$$

The maximum phase difference is observed when $d_1 - d_2$ is maximized. As thoroughly described in [20] and shown in Fig.

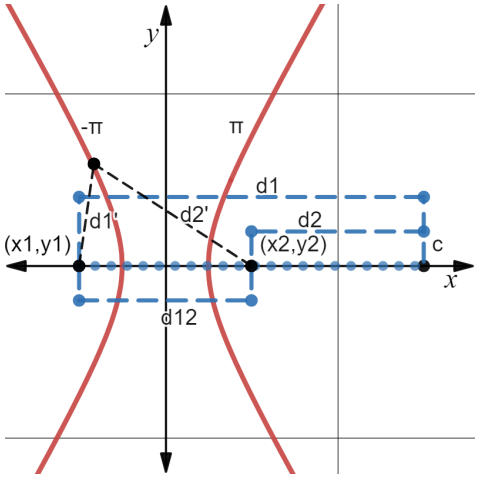

Fig. 1. Two antennas are located in (x_1, y_1) and (x_2, y_2) accordingly. Maximum phase difference is observed on the line connecting the two points where $d = d_1 - d_2 \Rightarrow d = d_{12}$.

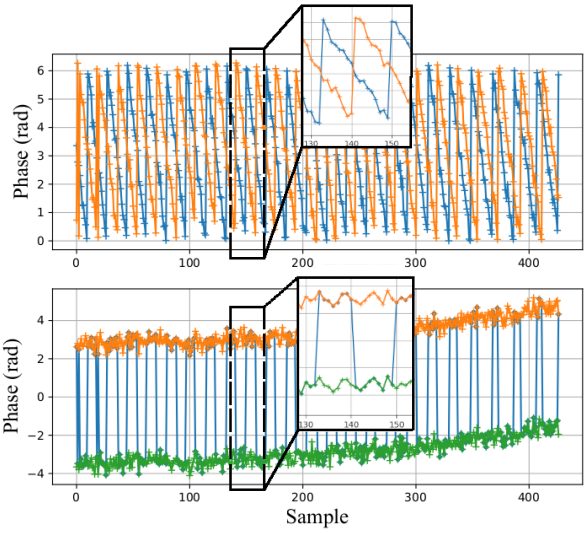

Fig. 2. Phase differences unwrapping and possible sequences

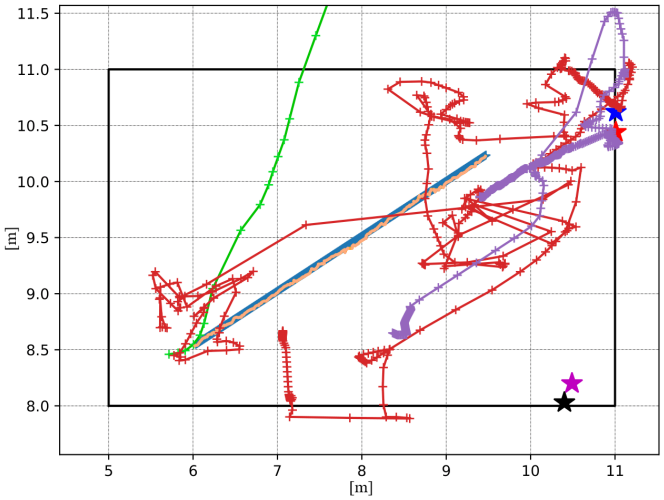

Fig. 3. Rejection of the wrong trajectories

1 this happens when the tag's position is on the line connecting the center of the two antennas (i.e. when $d_1 - d_2 = d_{12}$).

If $d_{12} = \lambda/2$ then the calculated phase difference ranges between -2π to 2π. In this work the distance between the antennas for each pair is considered less than $\lambda/2$.

2) Phase unwrapping : The majority of phase-based localization techniques use unwrapped phase data. Unwrapping is a time consuming procedure and not always accurate. If the measurements are not dense enough the unwrapping could fail leading to high estimation errors. Since our method exploits the phase difference, unwrapping of the raw data is not necessary. As shown in Fig. 2 though, some 2π jumps are noticed at the phase difference of the antenna pair due to the wrapping of the phase in $[0, 2\pi)$. The top plot shows the wrapped phase measurements collected from two antennas of the antenna-pair. The bottom plot shows the phase difference calculated. After correcting the 2π jumps the phase difference is shown in the bottom plot of Fig. 2 where the orange and green points are the two possible sequences after the correction.

3) Possible trajectories: After the 2π jumps' correction, an ambiguity remains since the time of arrival of each phase measurement is not known. This leads to two possible sequences of phase differences. In case of Fig. 2 the two sequences created can be seen with the orange and green color. The same ambiguity exists also on the other antenna pair, creating 4 possible combinations of sequences in total, hence 4 possible trajectories. At first all trajectories are calculated. Three trajectories are discarded either because they include points outside of the areas boundaries or because the include successive distant steps. Such an example can be seen in Fig. 3 where the real trajectory is represented by the blue points and the 4 calculated trajectories with orange, purple, red and green. Purple, red and green trajectories are exceeding the area boundaries (thick black lines) and at the same time present abnormal steps with respect to the time between successive measurements and are rejected. This process results to a single trajectory; i.e. the estimated one.

Since phase differences are bounded by the distance between the antennas of each pair a phase sequence could be rejected even before trajectory calculation. If there are values exceeding the phase difference limits the corresponding phase difference sequence is rejected, thus reducing the possible trajectories.

4) Phase noise: As (2) denotes, phase noise is Gaussian normally distributed with zero mean and variance σ^2_{phase}. In the proposed tracking method the entire search-space is mapped in measurements within [-2π, 2π], so a measurement phase error would result in large space-deviations. The effect of noise on the phase differences can be seen in Fig. 4 where phase data are derived from simulations. The blue line represents the noisy data derived from simulation. To avoid large errors a second degree Savitzky–Golay filter is applied to smooth the data and mitigate the phase-deviations. The orange line in Fig. 4 is the result of the filter being applied on the noisy phase differences. An alternative approach

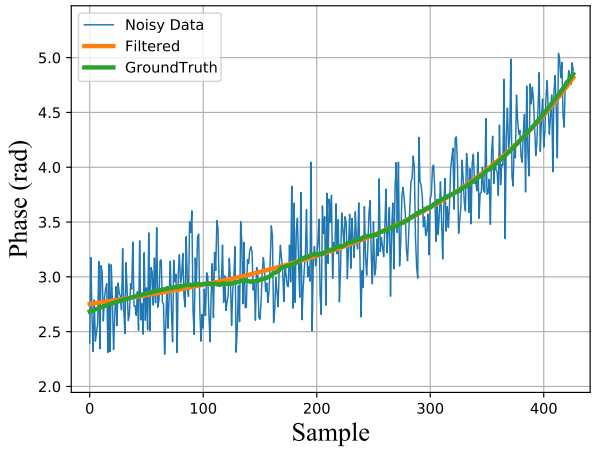

Fig. 4. Filtering of the noisy phase data.

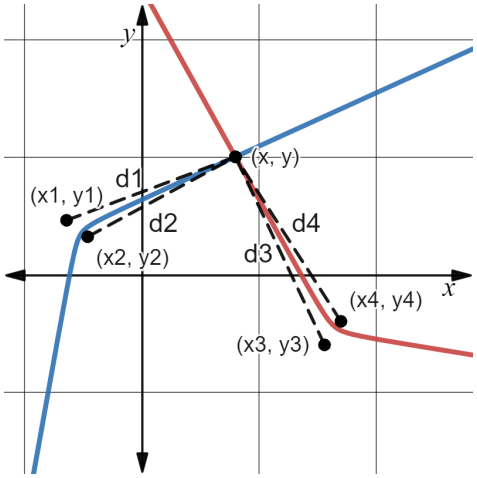

Fig. 5. Intersection of two hyperbolas' branches in the general case.

would be to exploit measured phase differences from largely spaced antennas, similarly to the principle introduced in [6]. This would result in many closely spaced hyperbolas; all representing the same phase difference (grating lobes). Under such conditions, the phase-error, due to noise, would result in a smaller shifting of the hyperbola and thus a smaller displacement error. However, the ambiguity, resulting from the cross section of multiple hyperbolas would greatly increase the complexity of the localization algorithm.

In these simulations the only factor of data deterioration taken into consideration is the Gaussian noise which is solved by filtering. In the experiments and real scenarios more factors of deterioration are present, such as multipath, insufficient collection of measurements, etc. In the corresponding measurements' section, these factors are further analyzed and ways to resolve them are presented.

B. Hyperbolas Intersection

Initially, let's assume an ideal multipath-free and noise-free environment, where ϕ_i is unwrapped and equal to ϕ_{prop}. Let also (x_i, y_i) be the position of each antenna i. The phase differences of the two antennas at each antenna pair are given by:

$$\Delta\phi_{12} = \frac{4\pi}{\lambda}(d_1 - d_2) \quad \text{and} \quad \Delta\phi_{34} = \frac{4\pi}{\lambda}(d_3 - d_4) \tag{7}$$

$$\Rightarrow \quad \Delta d_{12} = \frac{\lambda}{4\pi}\Delta\phi_{12} \quad \text{and} \quad \Delta d_{34} = \frac{\lambda}{4\pi}\Delta\phi_{34} \tag{8}$$

By substituting (4) in (8) we get:

$$||\mathbf{A}_{tag} - \mathbf{A}^1_{ant}||_2 - ||\mathbf{A}_{tag} - \mathbf{A}^2_{ant}||_2 = \frac{\lambda}{4\pi}\Delta\phi_{12} \tag{9}$$

$$||\mathbf{A}_{tag} - \mathbf{A}^3_{ant}||_2 - ||\mathbf{A}_{tag} - \mathbf{A}^4_{ant}||_2 = \frac{\lambda}{4\pi}\Delta\phi_{34} \tag{10}$$

As shown in Fig. 5 the loci of (9) and (10) are two hyperbolas intersecting in the actual position of the tag, assuming noiseless line of sight measurements.

Phase differences $\Delta\phi_{12}$ and $\Delta\phi_{34}$ are calculated from the phases of each antenna reported at the reader. To determine the position of the tag $\mathbf{A}_{tag}$ the system of equations (9) and (10) need to be solved. Trying to solve this system leads to sextic polynomials which cannot be solved with standard practices in the general case.

To overcome this problem and provide the algorithm with a robust and fast solution that calculates the tag's position with respect to the two phase-differences from two antenna-pairs a deep neural network is introduced. By providing the inputs (phase differences) and outputs (tag's positions), the neural network will try to fine tune its layers and weights so that the input best fits to the output. The trained neural network approximates the solution of the system of equations (9) and (10) and could be expressed as:

$$F_{NN}(\Delta\phi_{12}, \Delta\phi_{34}) = \mathbf{A}_{tag} \tag{11}$$

Notice here that in order for the NN to work, there must be a unique 1-to-1 mapping between the phase differences and the actual positions in the map. This assumption is always valid, provided that the NN is trained with the unwrapped theoretical phase differences that correspond to each position in the search area. If the antennas are spaced at distances smaller than $\lambda/2$, as in our case, then the measured data directly correspond to the expected theoretical data, under the constraints analyzed previously for the "Possible Trajectories". However, if the antennas are placed at greater distances, then an additional ambiguity is created, due to wrapping of the phase measurements and additional possible trajectories must be considered, which will be rejected if the target "moves" outside of the bounded physical area, as will be explained next.

C. Neural Network, Design and Training

The neural network is designed as a deep feed forward neural network (DFFNN). A DFFNN is basically a multilayer perceptron (MLP) and its main goal is to approximate a function. At the same time the hidden layers of a DFFNN are used to increase the non-linearity of the approximated function.

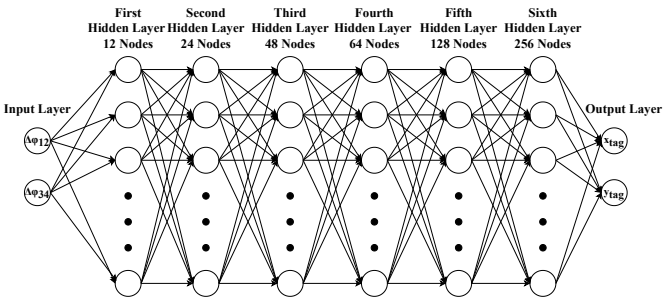

Fig. 6. The architecture of the Neural Network

A representation of the MLP designed, is shown in Fig. 6. The MLP consists of two input nodes ($\Delta\phi_{12}, \Delta\phi_{34}$), 5 hidden layers, each with different number of nodes, i.e. 12, 24, 48, 64, 128 and 256, respectively and two output nodes (x_{tag}, y_{tag}). A ReLu activation function was used for all layers and RMSProp for the optimizer. Moreover, a custom loss function that expresses the distance between the estimated position and the real one was applied and is given by:

$$Loss = ||\mathbf{A}_{tag\_real} - \mathbf{A}_{tag\_est}|| \tag{12}$$

The data set used for training, is generated via simulation and changes with respect to different arrangements of the antenna pairs and different size of spaces. Since we are interested in fixed installations, the data set needs to be trained once for each installation. For a given area, a dense grid of $1 \times 1mm^2$ is assigned and the theoretical values of the unwrapped phase differences for each antenna pair are calculated.

A trade-off between training speed and model accuracy with respect to the grid density is observed. Selecting a sparse grid, would lead to faster training of the neural network (less training data) but at the same time would inevitably result in lower accuracy. On the other hand a thick grid would offer higher model accuracy but would drastically increase the time of training. The size of $1\times1mm^2$ was selected as an acceptable compromise between those two.

During the training process either a small or even a zero percentage of the data is used as a validation data set, since there is no need for generalization. Leading the model to overfitting on the training data, achieves a better fitting on the desired function (11) and at the same time is used as an outliers' finder. As shown in II-A3, noisy or wrong input phase data will result to "non-logical" estimated positions, enhancing the tracking algorithm with the ability of distinction between measurements which originate from the given area and outliers.

D. Application in 3D Geometries and Large Inter-Antenna Spacing

The aforementioned process can be directly extended to random installations, involving 3D geometries. In general the two antennas, involved in the creation of a 3D hyperbola, could be positioned at different heights and at any distance among them. The solution is desired along a given plane; the target-tag's expected height. Notice that, under such 3D installations, the locus of the intersection of the 3D hyperbola, with the plane of the tag is not a 2D hyperbola; e.g. when the pair of antennas are located one on top of the other, the corresponding locus becomes circular. Under such general conditions the following steps must be taken:

- The user trains the NN on the specific height of the target tag with the physical-unwrapped phase values that would be collected on each antenna.
- During execution of the localization positioning algorithm, the user provides the trained NN all possible pairs of unwrapped phase differences that could exist for each pair of antennas: $\Delta\phi_{ij}(k) = \Delta\phi_{ij} + 2k\pi$; maximum k depends on the inter-antenna distance of each pair.
- The NN outputs different possible positions for each input pair of phase-differences. The NN will output points outside of the trained area, when the pair of phase-differences does not correspond to its trained geometry.
- The method then keeps track of all possible trajectories, by fixing k for each initially considered phase difference and unwrapping the corresponding $\Delta\phi_{ij}(k)$.

III. Simulations

In this section the proposed algorithm is validated in simulated geometries. The training process is evaluated with respect to the given area size and the arrangement of the antennas. The training time and accuracy of the model are evaluated. The mean error of the estimations is calculated for different paths:

$$Error = \frac{\sum_{n=1}^{N} ||\mathbf{A}^n_{tag\_est} - \mathbf{A}^n_{tag\_real}||_2}{N} \tag{13}$$

A. Neural Network Training, Time and Accuracy

For each antenna arrangement and given area a different geometrical model is trained. The training time of the neural network depends on the size of the area, the grid density and the desired localization accuracy. The search area is a 3x6 m^2 room with the antennas positioned at the star points, as shown in Fig. 7. The error for each grid point is calculated as $||\mathbf{A}^i_{tag\_est} - \mathbf{A}^i_{tag\_real}||_2$ and a color mesh plot is created for different number of training epochs. As shown in Fig. 7 the neural network keeps converging to the desired function as the epochs increase. The training process is interrupted when a predefined threshold of mean error is passed ($\mu_{error} < 0.02m$). The standard deviation (std) of the error should be kept low ($\sigma^2_{error} < 0.01m$).

Four different arrangements of antennas are shown: A) 3 antennas in a line forming 2 antenna pairs, B) 4 antennas in a line, forming 2 antenna pairs, C) 2 antenna pairs perpendicular to each other and D) 2 antenna pairs with non-perpendicular orientation. For each arrangement a neural model was trained for 5000 epochs and the results can be seen in Fig. 8. In cases A-C, there are some areas, where the model appears poorly trained. This effect takes place at positions, where the hyperbolas cross at shallow angles (the lines of the hyperbolas are nearly parallel). In arrangement A and B this property affects larger regions due to the fact that both pairs are co-linear. In arrangement C, the region of poor training lies near

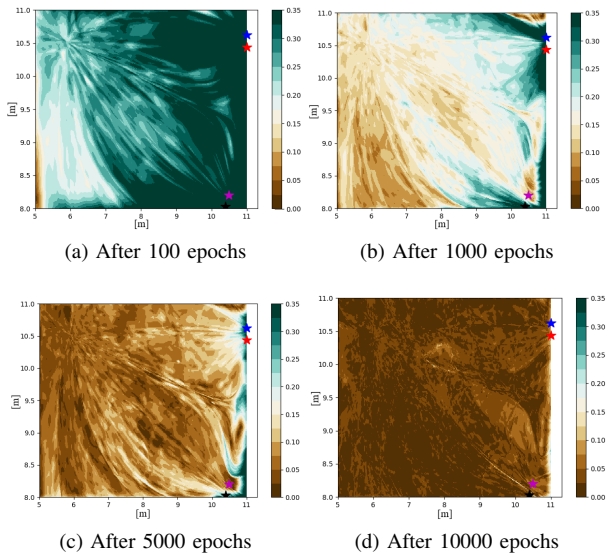

(a) After 100 epochs (b) After 1000 epochs

(c) After 5000 epochs (d) After 10000 epochs

Fig. 7. The star points represent the position of the antennas. The given area is a $3x6m^2$ room and the localization error of each grid point is calculated and mapped as depicted in the colormap. The accuracy of the model improves at increasing epochs.

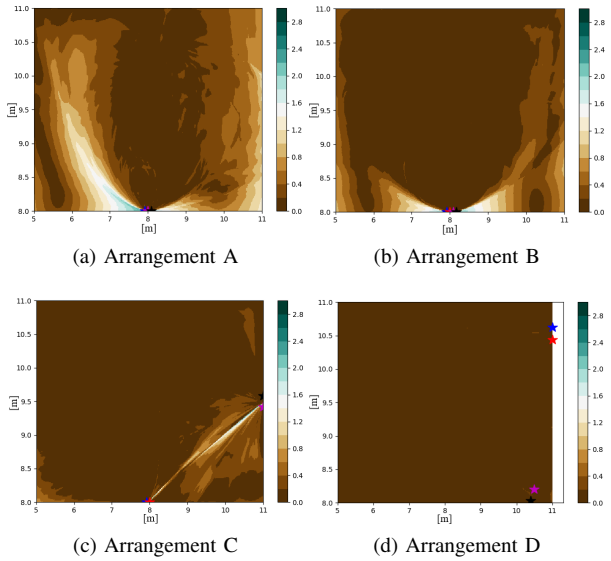

(a) Arrangement A (b) Arrangement B

(c) Arrangement C (d) Arrangement D

Fig. 8. Result of training of the neural model for 5000 epochs and 4 different antenna arrangements respectively.

the line connecting the center of the two pairs. This effect is eliminated in arrangement D, where the axes of the foci of the two hyperbolas are such, that the hyperbolas do not cross at shallow angles for any point in the search area. Consequently this effect affects the training and the whole system's accuracy.

B. Trajectory Tracking, Simulated Paths

A neural network was trained for a specific area and a given antenna pair formation. Different paths were simulated and the accuracy of the tracking algorithm was evaluated using (13). A 3x6 m^2 area is chosen and the 2 antenna pairs have the orientation of arrangement D. A top view of the setup and the simulated paths can be seen in Fig. 9. The 4 stars represent

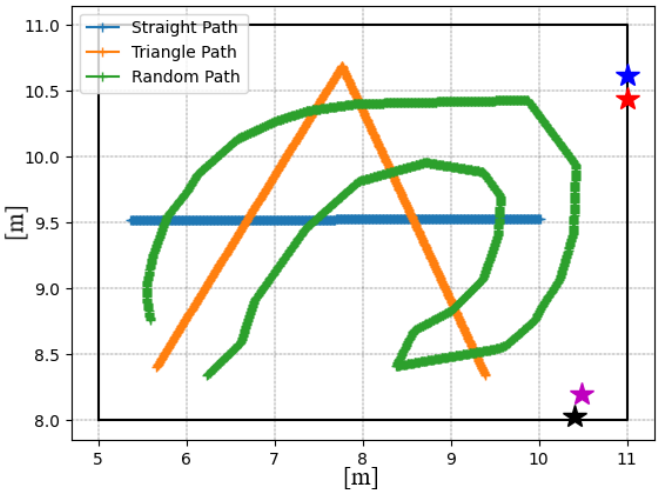

Fig. 9. Top view of the simulation setup and the simulated trajectories.

TABLE I
SIMULATION RESULTS

Paths	Mean Error(m)	Standard Deviation(m)
Straight Path	0.05	0.03
Triangle Path	0.07	0.05
Random Path	0.06	0.05

the position of the 4 antennas and orange, blue and green lines represent the 3 different simulated paths.

For each trajectory, phase data of each antenna are simulated as denoted in (1). Phase differences are calculated and filtered for each antenna pair and the 4 possible trajectories are created. The algorithm rejects the wrong paths as shown in II-A3 and the error between the estimated trajectory and the ground truth is calculated for each path.

The results can be seen in Table I. In all paths, the phase differences were filtered using a Savitzky–Golay filter before feeding them to the trained model. Unfiltered phase differences, lead to larger errors, reaching values up to 1 meter, depending on σ^2_{noise}. In Fig. 10 an estimation of the random trajectory both with filtered and unfiltered data is presented. Filtered vs unfiltered phase differences were passed through the trained model and the estimated positions are plotted with green and blue lines accordingly. The orange line represents the ground truth. Also in Fig. 10 a relation between the distance of the target from the antenna pairs and the accuracy of the results is shown. In the left side of the plot (i.e. maximum distance between target and antennas) mean error is higher versus a search region closer to the two antenna pairs. This effect is observed for any antenna arrangement as in greater distances from the antennas, a small error in the measured phase-difference would result in a larger error in the position of the intersection point of the two hyperbolas, compared to the same phase-difference error in smaller distances.

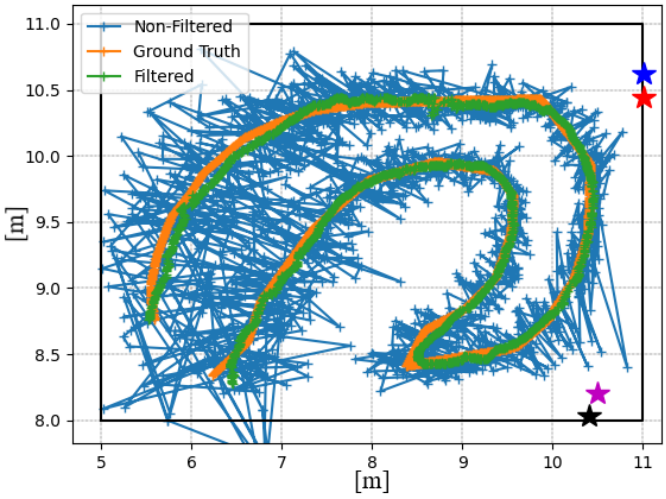

Fig. 10. Location estimations of the neural model when unfiltered phase data are used as an input versus estimations when input phase data are filtered.

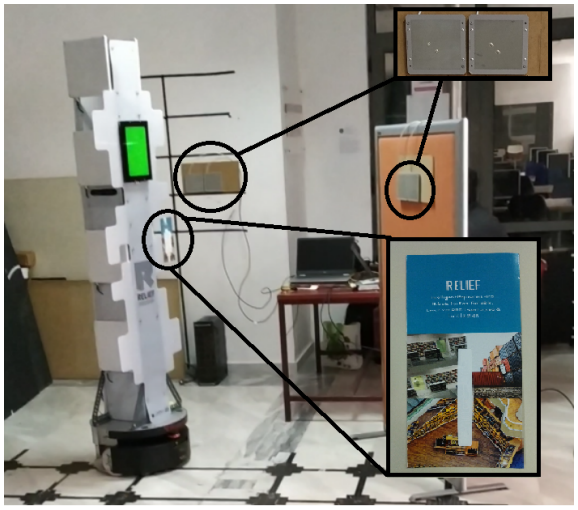

Fig. 11. The setup of the experiments. The tag is placed on a SLAM-capable robot. The two antenna pairs are placed at known locations and the two antennas per pair are placed at a distance less than $\lambda/2$.

IV. Experimental Results

The proposed algorithm is experimentally evaluated in different setups. Initially, experiments take place using a tagged robot capable of performing SLAM. The next set of experiments are carried out by RFID-tagged people in a multipath rich laboratory-environment. Finally, we discuss on factors which may have a negative effect on the performance of the tracking algorithm.

A. Experiments with a Tagged Robot

The experiments were conducted in a $6{\times}8m^2$ lab of the school of Electrical and Computer Engineering of the Aristotle University of Thessaloniki. The tag was mounted on a robot that estimates its pose at cm accuracy, thanks to a lidar-sensor, combined with its odometry-sensors and Kalman filtering. The robot's pose is used as the ground truth of the position of the tag. Then, the error between the estimated and the real position can be calculated (13).

The setup of the experiments can be seen in Fig. 11. An Alien ALN-9740 "Squiggle" tag was used as the target tag with a sensitivity of -19 dBm. The Impinj Speedway R420 reader and four Laird PER86506 antennas were used, to collect phase data measurements . The two antennas per pair are placed at a distance less than $\lambda/2$. One of the antenna pairs is placed on a fixed position on the wall and the other on a stand that can change positions, thus enabling experiments with different antenna arrangements.

The map created by the robot and the trajectories traversed are presented in Fig. 12. During the blue and green path the robot kept a constant speed. The red and orange paths of the robot represent an abstract movement to imitate a human's random trajectory . During these two paths the robot decelerates, accelerates, stops and rotates arbitrarily.

Initially, the neural model is trained, given the arrangement and area of interest. The neural model is trained until a threshold of mean error $\mu_{error} < 0.02m$ and standard deviation $\sigma^2_{error} < 0.01m$ is reached.

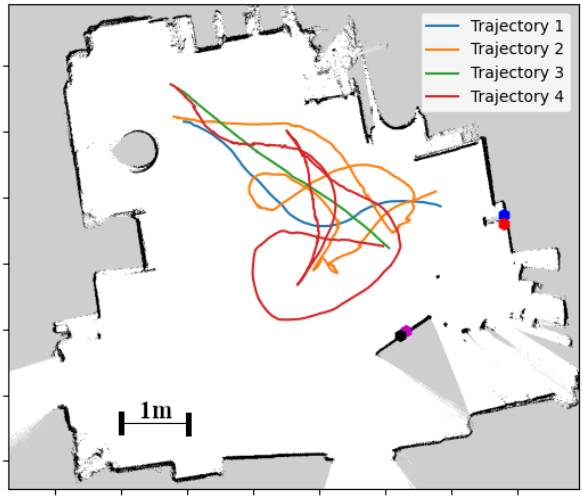

Fig. 12. The four trajectories traversed by the tag on the robot during experiments. The green and blue path are two paths without stops and changes on the speed of the robot while the orange and red path imitate a human movement as the robot decelerates, turns arbitrarily and performs stops along the route followed.

In Fig. 13 the tracking algorithm is presented step by step. The trajectory #4 is selected since it is more representative of a human's behavior. At first the RFID reader reports phase measurements from each antenna. The measurements are not collected at the same time for each antenna; thus calculating the phase differences per antenna pair is not a straightforward process. To calculate the phase differences between the antennas a "common" time series is generated according to the time instances of the raw phase measurements. The common time instances are generated via linear interpolation at time slots where a high read rate per tag is observed. If interpolation process fails for a time window of even one of the antennas then this time window is excluded from the tracking algorithm. The result of this process is shown in Fig. 13a where the raw data are presented with blue color and the interpolated with

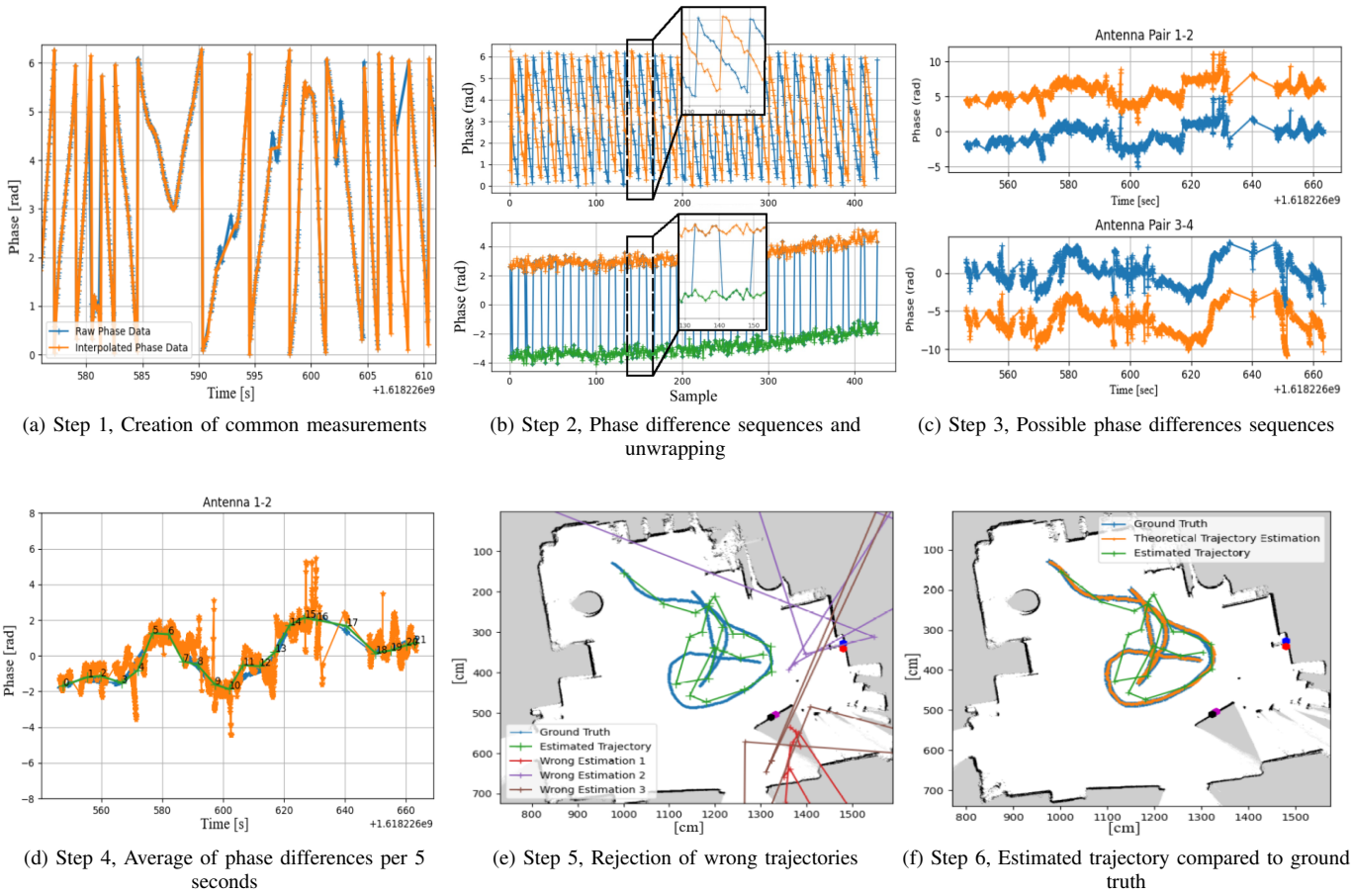

(a) Step 1, Creation of common measurements

(b) Step 2, Phase difference sequences and unwrapping

(c) Step 3, Possible phase differences sequences

(d) Step 4, Average of phase differences per 5 seconds

(e) Step 5, Rejection of wrong trajectories

(f) Step 6, Estimated trajectory compared to ground truth

Fig. 13. Steps of the tracking algorithm.

orange.

Then, the phase differences are calculated and the unwrapping process takes place as presented in II-A3 and shown in Fig. 13b. The phase data collected are wrapped. As a result, the sign of the collected phase difference is ambiguous. Given that the distance between the antennas on each pair is less than $\lambda/2$ and that the order of arrival of each phase measurements is unknown two possible phase difference sequences are generated for each antenna pair. The same ambiguity exists also on the other antenna pair, creating 4 possible combinations of sequences in total, hence 4 possible trajectories. In case of Fig. 13c the two possible sequences for antenna pair 1-2 and 3-4 can be seen with the orange and blue color in the two subplots respectively.

At this stage during simulations the data were filtered using a Savitzky–Golay filter assuming that distortion on the phase measurements only derives from Gaussian noise. By observing the phase difference sequences we notice that the effect of multipath is significantly high and affects the data for more than just an instance. For that reason just filtering the sequence would not solve the issue. To overcome this problem an average of consecutive phase measurements in a time window of 5 seconds is calculated (Fig. 13d).

The four phase difference sequences generate four possible trajectories after passing through the trained model. The trajectories that either exceed the area's boundaries or present steps bigger than a human could possible perform during 5 seconds, are rejected (red, brown and purple paths in Fig. 13e). After the trajectory rejection process, the final estimated trajectory is presented in Fig. 13f presenting a mean error of 0.47m. The results of all four trajectories can be seen in Table II.

TABLE II
ROBOT EXPERIMENT RESULTS

Paths	Mean Error(m)	Standard Deviation(m)
Trajectory 1	0.32	0.22
Trajectory 2	0.37	0.28
Trajectory 3	0.24	0.17
Trajectory 4	0.47	0.33

B. Experiments with Tagged Human

Experiments where the tag is placed on a human were conducted, in order to investigate the effect of human body on the phase measurements and also the accuracy of the method in real life scenarios. The experiments took place in a School's lab, filled with desks and desktop computers, thus creating a "multipath-rich" environment.

The setup of the experiments can be seen in Fig. 14. An Alien ALN-9740 "Squiggle" tag was used as the target tag while the Impinj Speedway R420 reader collected the phase

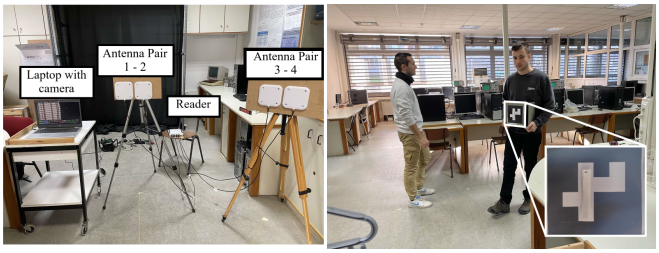

(a) Hardware Equipment (b) Human carrying tag

Fig. 14. The setup of the experiments with a tagged human.

measurements via four A5020 circularly polarized antennas manufactured by Times-7. The two antenna-pairs were set with non-perpendicular orientation (Arrangement D in Fig. 8) using two tripods as shown in Fig. 14a. For each pair, the distance between the two antennas was kept less than $\lambda/2$.

The trajectories followed by the human are shown in Fig. 15. In trajectories 1-3 the person reaches a point and returns back imitating a museum visitor approaching an exhibit and then moving away to continue his visit. To examine the proposed method in the presence of human and other tagged persons trajectory #2 is almost identical to trajectory #3 but a second tagged person is wandering at the search area as shown in Fig. 14b. Trajectory #4 imitates an arbitrary movement of a human.

ArUco markers are used, in order to acquire the ground truth of the tag's/human's position, by means of a visual system. ArUco is a library for detection of square fiducial markers developed by R. Muñoz and S. Garrido [23]. Such a square marker (i.e. ArUco marker) is carried by the person who follows the trajectories. The tag is placed on top of the ArUco marker (Fig. 14b) in such a manner that it does not alter the shape of the marker, while ensuring that their position is the same. A laptop equipped with a camera (see Fig. 14a) is set next to the antenna pairs and detects the marker's position with high accuracy (i.e. mean error less than 1cm) in space, thus acquiring the tag's position during the experiments. The tag's location estimations of the proposed algorithm are compared with the marker's location provided by the visual detection system.

The tracking algorithm is applied as described in IV-A for all trajectories and the error between the estimated trajectory and the ground truth is given by (13). Kalman filtering is applied, to refine the precision of the estimations. The mean and standard deviation for each case can be seen in Table III and a plot of estimations versus ground truth is shown in Fig. 16.

The mean error remains under 0.5m for all trajectories followed. The effect of another tagged person in the search space is observed in Trajectory #3 with respect to Trajectory #2, as a slight increase in the mean error and standard deviation. Kalman filtering has a small effect on the mean error and std of the experiments and that is due to the fact that the collected phase measurements have already been filtered and averaged over larger time-segments, thus do not present large variations. However, visually, Kalman filtering results

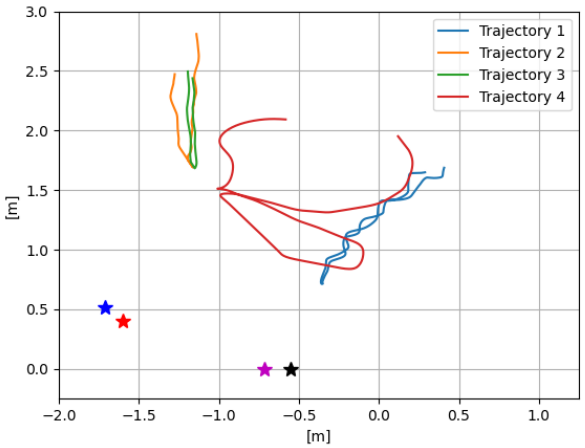

Fig. 15. The four trajectories followed by the human. Top View.

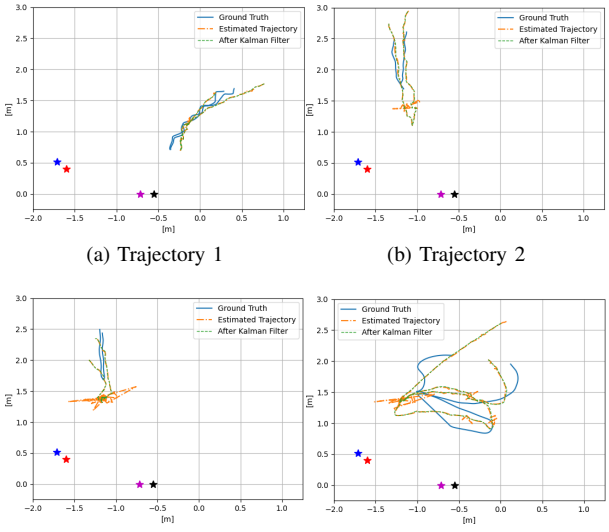

(a) Trajectory 1 (b) Trajectory 2

(c) Trajectory 3 (d) Trajectory 4

Fig. 16. Location estimations before and after Kalman Filters compared to ground truth for all trajectories.

in a much smoother trajectory that resembles a real human movement, as shown in Fig. 16. Notice that the green-trace (Kalman-filtered) no longer suffers by the variations shown in the orange trace.

TABLE III
HUMAN EXPERIMENT RESULTS

Paths	Initial Estimations		After Kalman	
	Mean Error(m)	Std(m)	Mean Error(m)	Std(m)
Trajectory 1	0.25	0.19	0.25	0.17
Trajectory 2	0.40	0.25	0.40	0.21
Trajectory 3	0.45	0.3	0.43	0.27
Trajectory 4	0.31	0.24	0.30	0.22

C. Factors that Affect the Tracking Algorithm

The algorithm developed in this work is able to track moving tags using antennas at fixed positions. The main goal is to track RFID-tagged visitors inside a museum.

A new challenge arises, since the visitors need to be tagged. Dielectric-spacers between the tag and the human body may be needed to avoid detuning of the tag's antenna. In [24], the authors propose techniques to attach tags even to conductive materials with the use of slim insulating materials. Such insulating materials could be used to manufacture RFID equipped wristbands or cardholder neck straps that will not affect the readability of the tag even in close proximity to the human body. Nevertheless, there will always be areas where the tag to reader link will be blocked from the visitor's body. This will lead to intermittent sequences of phase measurements. Stationary motion and high velocity is also expected to affect the collection of phase measurements. Stationary motion of the visitors body will look like noise and will be filtered out in pre or post processing. High velocities will lead to low read rates per antenna per tag and might affect the tackling of multipath. This problem is solved by dividing the measurements to independent trust intervals. The difficulty lies on the "connection" of these intervals, where Kalman filtering would assist on smoothing the curves and minimizing the mean error. Furthermore, at least two tags will be attached to each ticket, thus ensuring diversity in the collected measurements; this is expected to improve the detection period per visitor.

Phase measurements are also affected by the change of the corresponding RSSI measurements. As described in [25] variations of the incident power on the tag might lead significant phase-shifts (measured as high as 100^o). In our case phase differences between adjacent antennas are exploited. If the variations of the incident power at the tag are similar then the effect on phase differences would be negligible. On the other hand if the fading pattern for each antenna is different, then the phase shift per antenna would alter the phase differences accordingly. This problem is also treated thanks to the time-averaging window; position-estimations are the results of phase-difference averages over larger time-windows.

Fluctuations in signal strength and phase measurements were observed both in the robot and the human experiments due to multipath. The areas, where the experiments took place, are multipath-rich indoor environments. Again, filtering and averaging of the raw phase-difference data was proven to be sufficient to tackle the fast-changing effect of multipath. Larger positioning-errors were observed only when a systematic error was introduced in the phase-difference measured data (e.g. phase deviation for several seconds - larger than the averaging window). This could be the effect of an electromagnetically-strong scatterer (e.g. a metallic closet); under such conditions the positioning error could be larger than 0.5m. Such an effect cannot be detected by the proposed method.

V. Conclusion

Real-time tracking of moving targets is a key feature for Industry 4.0 applications. In this paper we present a novel method on tracking a UHF-RFID tagged target in real time. The method exploits neural networks to track a moving UHF-RFID tag via hyperbolic positioning. The proposed neural model needs to be trained only once for each antenna-geometry installation. It is trained until reaching low values of mean error and std. A priori knowledge of initial position of the target is not needed. The tracking method will be used to track visitors inside a museum and quantify their behavior, but can be applied for different cases. Two type of experiments were conducted: *i*) by placing a tag on a moving robot which imitates a visitor's behavior by moving arbitrarily and *ii*) by placing it on an ArUco Marker carried by a human. Experimental results showed a mean error of under 0.5m throughout the campaign.

Future work will include different environments and larger tag populations to test the robustness of the algorithm in different multipath conditions.

References

[1] T. Kanda, M. Shiomi, L. Perrin, T. Nomura, H. Ishiguro and N. Hagita, "Analysis of People Trajectories with Ubiquitous Sensors in a Science Museum," Proceedings IEEE International Conference on Robotics and Automation, pp. 4846-4853, 2007, doi: 10.1109/ROBOT.2007.364226.

[2] A. R. Jimenez Ruiz, F. Seco Granja, J. C. Prieto Honorato and J. I. Guevara Rosas, "Accurate Pedestrian Indoor Navigation by Tightly Coupling Foot-Mounted IMU and RFID Measurements," in IEEE Transactions on Instrumentation and Measurement, vol. 61, no. 1, pp. 178-189, Jan. 2012, doi: 10.1109/TIM.2011.2159317.

[3] M. Omer, G. Y. Tian, "Indoor distance estimation for passive UHF RFID tag based on RSSI and RCS," Measurement, Volume 127, pp. 425-430, 2018, doi:10.1016/j.measurement.2018.05.116.

[4] Y. Zhang, M. G. Amin, S. Kaushik, "Localization and Tracking of Passive RFID Tags Based on Direction Estimation," International Journal of Antennas and Propagation, vol. 2007, doi: 10.1155/2007/17426.

[5] S. Azzouzi, M. Cremer, U. Dettmar, R. Kronberger and T. Knie, "New measurement results for the localization of UHF RFID transponders using an Angle of Arrival (AoA) approach," 2011 IEEE International Conference on RFID, 2011, pp. 91-97, doi: 10.1109/RFID.2011.5764607.

[6] J. Wang, D. Vasisht, and D. Katabi. 2014. RF-IDraw: virtual touch screen in the air using RF signals. In Proceedings of the 2014 ACM conference on SIGCOMM (SIGCOMM '14). Association for Computing Machinery, New York, NY, USA, 235–246. doi: 10.1145/2619239.262633

[7] X. Lu, L. Wang, D. Zhao and C. Zhai, "Multi-tag RFID system enables localization and tracking," Journal of Physics: Conference Series, vol. 1168, 2019, doi:10.1088/1742-6596/1168/2/022103.

[8] S. Sarkka, V. V. Viikari, M. Huusko and K. Jaakkola, "Phase-Based UHF RFID Tracking With Nonlinear Kalman Filtering and Smoothing," in IEEE Sensors Journal, vol. 12, no. 5, pp. 904-910, May 2012, doi: 10.1109/JSEN.2011.2164062.

[9] C. Jiang, Y. He, X. Zheng and Y. Liu, "Orientation-Aware RFID Tracking with Centimeter-Level Accuracy," 2018 17th ACM/IEEE International Conference on Information Processing in Sensor Networks (IPSN), 2018, pp. 290-301, doi: 10.1109/IPSN.2018.00057.

[10] L. Yang, Y. Chen, X. Y. Li, Ch. Xiao, Mo Li and Y. Liu, "Tagoram: Real-time Tracking of Mobile RFID tags to High Precision Using COTS Devices," 2014, 20th Annual International Conference on Mobile Computing and Networking (MobiCom '14), 2014, pp 237–248, doi: 10.1145/2639108.2639111.

[11] A. Raptopoulos Chatzistefanou, A. Tzitzis, S. Megalou, G. Sergiadis and A. G. Dimitriou, "Trajectory-Tracking of UHF RFID Tags, Exploiting Phase Measurements Collected From Fixed Antennas," in IEEE Journal of Radio Frequency Identification, vol. 5, no. 2, pp. 191-206, June 2021, doi: 10.1109/JRFID.2021.3053101.

[12] M. Scherhäufl, M. Pichler, E. Schimbäck, D. J. Müller, A. Ziroff and A. Stelzer, "Indoor Localization of Passive UHF RFID Tags Based on Phase-of-Arrival Evaluation," in IEEE Transactions on Microwave Theory and Techniques, vol. 61, no. 12, pp. 4724-4729, Dec. 2013, doi: 10.1109/TMTT.2013.2287183.

[13] Z. Chen, P. Yang, J. Xiong, Y. Feng and X. -Y. Li, "TagRay: Contactless Sensing and Tracking of Mobile Objects using COTS RFID Devices," IEEE INFOCOM 2020 - IEEE Conference on Computer Communications, 2020, pp. 307-316, doi: 10.1109/INFOCOM41043.2020.9155531.

[14] J. Wang, J. Xiong, H. Jiang, X. Chen and D. Fang, "D-Watch: Embracing "Bad" Multipaths for Device-Free Localization With COTS RFID Devices," in IEEE/ACM Transactions on Networking, vol. 25, no. 6, pp. 3559-3572, Dec. 2017, doi: 10.1109/TNET.2017.2747583.
[15] L. Yang, Q. Lin, X. Li, T. Liu, and Y. Liu. "See Through Walls with COTS RFID System!" In Proceedings of the 21st Annual International Conference on Mobile Computing and Networking (MobiCom '15). Association for Computing Machinery, New York, NY, USA, pp. 487–499, 2015, doi: 10.1145/2789168.2790100.
[16] Y. Ma, W. Ning, B. Wang and X. Liang, "A Data Augmentation-Based Method for Robust Device-Free Localization in Changing Environments of Passive Radio Frequency Identification System," in IEEE Transactions on Instrumentation and Measurement, vol. 70, pp. 1-13, 2021, Art no. 8003013, doi: 10.1109/TIM.2021.3065426.
[17] D. Zhang, J. Ma, Q. Chen and L. M. Ni, "An RF-Based System for Tracking Transceiver-Free Objects," Fifth Annual IEEE International Conference on Pervasive Computing and Communications (PerCom'07), 2007, pp. 135-144, doi: 10.1109/PERCOM.2007.8.
[18] D. Zhang et al., "Fine-Grained Localization for Multiple Transceiver-Free Objects by using RF-Based Technologies," in IEEE Transactions on Parallel and Distributed Systems, vol. 25, no. 6, pp. 1464-1475, June 2014, doi: 10.1109/TPDS.2013.243.
[19] H. Ma, Y. Wang, K. Wang and Z. Ma, "The Optimization for Hyperbolic Positioning of UHF Passive RFID Tags," in IEEE Transactions on Automation Science and Engineering, vol. 14, no. 4, pp. 1590-1600, Oct. 2017, doi: 10.1109/TASE.2017.2656947.
[20] T. Liu, Y. Liu, L. Yang, Y. Guo and C. Wang, "BackPos: High Accuracy Backscatter Positioning System," in IEEE Transactions on Mobile Computing, vol. 15, no. 3, pp. 586-598, 1 March 2016, doi: 10.1109/TMC.2015.2424437.
[21] P. Tripicchio, M. Unetti, S. D'Avella, A. Buffi, A. Motroni, F. Bernardini and P. Nepa "A Synthetic Aperture UHF RFID Localization Method by Phase Unwrapping and Hyperbolic Intersection," in IEEE Transactions on Automation Science and Engineering (Early Access), 19 February 2021, doi: 10.1109/TASE.2021.3057433.
[22] P. V. Nikitin, R. Martinez, S. Ramamurthy, H. Leland, G. Spiess and K. V. S. Rao, "Phase based spatial identification of UHF RFID tags," 2010 IEEE International Conference on RFID (IEEE RFID 2010), 2010, pp. 102-109, doi: 10.1109/RFID.2010.5467253.
[23] S. Garrido-Jurado, R. Muñoz-Salinas, F. J. Madrid-Cuevas and M. J. Marín-Jiménez, "Automatic generation and detection of highly reliable fiducial markers under occlusion", Pattern Recognition vol. 47, 6 June 2014, pp. 2280-2292. doi: 10.1016/j.patcog.2014.01.005
[24] M. Dermenoudi, D. Karolidis, A. Moneda, V. Drakaki and A. Dimitriou, "The Use of RFID Technology for the Collection Management in the Archaeological Museum of Thessaloniki," 2021 6th International Conference on Smart and Sustainable Technologies (SpliTech), 2021, pp. 01-06, doi: 10.23919/SpliTech52315.2021.9566423.
[25] S. Megalou, A. Bletsas, T. Yioultsis and A. G. Dimitriou, "Power and Phase Variation of Backscattered RFID Signal with Respect to the Incident Power at the Tag," 2021 IEEE International Conference on RFID Technology and Applications (RFID-TA), 2021, pp. 36-39, doi: 10.1109/RFID-TA53372.2021.9617367.

Spyros Megalou received the MSc degree in Electrical and Computer engineering from the Aristotle University of Thessaloniki, Greece, in 2019, and he is currently pursuing the PhD degree at the same School. His main research interests include RFID technology, localization techniques, microwave applications and antenna design. He is also a member of a space related group (BEAM, Beyond Earth Aristotle Missions) focusing on space experiments and applications.

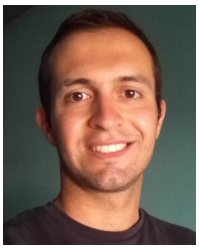

Aristidis Raptopoulos Chatzistefanou was born in Florina, Greece, in 1996. He received the Diploma degree in electrical and computer engineering from the Aristotle University of Thessaloniki in 2019, where he is currently pursuing the Ph.D. degree, and working as a Research Assistant with the Aristotle University of Thessaloniki. His main research interests include RFID technology, localization and tracking techniques.

Anastasios Tzitzis was born in Thessaloniki, Greece, in 1994. In 2018 he received the Diploma in Electrical and Computer Engineering from Aristotle University of Thessaloniki, where he is currently working toward the Ph.D. degree. At the same time, he is working as a Research and Teaching Assistant at the Aristotle University. His current research interests include analysis and design of antennas, RFID technology and wave propagation.

Traianos V. Yioultsis (M'09) received the Diploma and the Ph.D. degrees in electrical and computer engineering from the Aristotle University of Thessaloniki, Greece, in 1992 and 1998, respectively. From 2001 to 2002, he was a Post-Doctoral Research Associate with the Department of Electrical and Computer Engineering, University of Illinois at Urbana–Champaign. Since 2002, he has been with the Department of Electrical and Computer Engineering, Aristotle University of Thessaloniki, where he is currently a Professor. His current interests include the analysis and design of antennas and microwave circuits with fast computational techniques, and the modeling of complex wave propagation problems. He has also served as a member of the Editorial Board for IEEE Communications Letters and several international conferences.

Antonis G. Dimitriou (S'01-M06-SM'14) received the diploma and the Ph.D degree in Electrical and Computer Engineering from the Aristotle University of Thessaloniki, Greece, in 2001, and 2006 respectively. Since 2007, he is with the School of Electrical and Computer Engineering of AUTh, where he currently serves as a teaching and research faculty member.

He has participated in more than 20 research projects, 8 of which since 2007 as a principal investigator in the fields of Robotics, RFIDs, and Wireless Sensor Networks. He is currently the coordinator of project "RELIEF", involving continuous RFID inventorying through robotics and project "CULTUREID", where RFID equipment is installed inside the Archaeological Museum of Thessaloniki to monitor RFID tagged exhibits and track visitors. He was a Management Committee Member in the ICT COST Action IC301 "Wireless Power Transmission for Sustainable Electronics (WiPE)". He is the author or co-author of approximately 70 journal and conference papers.

Dr. Dimitriou was the recipient of the Ericsson Award of Excellence in Telecommunications in 2001 and co-recipient of the student-paper award in the 2011 IEEE RFID-TA conference. He received the "IEEE Wireless Communications Letters Exemplary Reviewer" award in 2012 and 2014. He is a Senior IEEE Member since February 2014. Since 2021, he serves as a vice-chair in the IEEE Technical Committee on Motion Capture and Localization. He also serves as a reviewer for major journals and TPC member for major conferences.